Reversible Pressure-Magnetic Modulation in a Tetrathiafulvalene-Based Dyad Piezochromic Dysprosium Single-Molecule Magnet

Fabrice Pointillart, Jessica Flores Gonzalez, Haiet Douib, Vincent Montigaud, Charles J. Mcmonagle, Boris Le Guennic, Olivier Cador, Dawid Pinkowicz, Michael R. Probert

Reversible Pressure-Magnetic Modulation in a Tetrathiafulvalene-Based Dyad Piezochromic Dysprosium Single-Molecule Magnet

Fabrice Pointillart,*[a] Jessica Flores Gonzalez,[a] Haiet Douib,[a] Vincent Montigaud,[a] Charles J. McMonagle,[b] Boris Le Guennic,*[a] Olivier Cador,[a] Dawid Pinkowicz*[c] and Michael R. Probert[b]

[a] Dr. F. Pointillart, Dr. J. Flores Gonzalez, Dr. H. Douib, V. Montigaud, Dr. B. Le Guennic, Prof. O. Cador
Univ Rennes, CNRS, ISCR (Institut des Sciences Chimiques de Rennes) - UMR 6226, F-35000 Rennes, France.
E-mail : fabrice.pointillart@univ-rennes1.fr, boris.leguennic@univ-rennes1.fr

[b] Dr. C. J. McMonagle, Prof. M. R. Probert
Chemistry, School of Natural and Environmental Sciences, Newcastle University, Newcastle upon Tyne, NE1 7RU, United Kingdom

[c] Dr. D. Pinkowicz
Faculty of Chemistry, Jagiellonian University, Gronostajowa 2, 30-387 Kraków, Poland.
E-mail : dawid.pinkowicz@uj-edu.pl

Supporting information for this article is given via a link at the end of the document.

Abstract: The extreme sensitivity of trivalent lanthanide ions to crystal field variations led to the emergence of single-molecule magnetic switching under various stimuli. The use of pressure as an external stimulus instead of classic light irradiation, oxidation or any chemical reactions allows a fine tuning of the magnetic modulation. Here the well-known pure isotopically enriched $[^{162}Dy(tta)_3(\mathbf{L})]\cdot C_6H_{14}$ (**^{162}Dy**) Single-Molecule Magnet (SMM) (tta^- = 2-2-thenoyltrifluoroacetonate and **L** = 4,5-bis(propylthio)-tetrathiafulvalene-2-(2-pyridyl)benzimidazole-methyl-2-pyridine) was experimentally investigated by single-crystal diffraction and squid magnetometry under high applied pressures. Both reversible piezochromic properties and pressure modulation of the slow magnetic relaxation behavior were demonstrated and supported by ab initio calculations. The magnetic study of the diluted sample $[^{162}Dy_{0.05}Y_{0.95}(tta)_3(\mathbf{L})]\cdot C_6H_{14}$ (**^{162}Dy@Y**) indicated that variations in the electronic structure have mainly intermolecular origin with weak intramolecular contribution. Quantitative magnetic interpretation concludes to a deterioration of the Orbach process for the benefit of both Raman and QTM mechanisms under applied pressure.

Introduction

In the context of systems suitable for potential applications in high density data storage, the discovery of the Single-Molecule Magnet (SMM) behaviour for a cluster of twelve manganese ions[1-2] paved an exciting research way in the molecular magnetism field. The difficulties to push the boundaries of the performances due to the equilibrium between magnetic anisotropy and spin values associated to the discovery of the first mononuclear lanthanide SMM,[3] this led to a virtual monopoly for lanthanide chemistry in the design of high performance SMMs.[4-8] The use of computational approaches to better understand the needed prerequisites helped to optimize such systems.[9-10] Thus the strong uniaxial magnetic anisotropy observed in organometallic lanthanide complexes allowed the observation of a high blocking temperature, up to 80 K.[11-14] Such molecular systems which display magnetic bistability could become good candidates to applications such as quantum computing[15] and spintronics.[16] With the aim to extend the range of potential applications dedicated to SMMs, the reversible modification of the magnetic behaviour by applying external stimuli opens the possibility to design switches and sensors.[17] The switching of SMM behaviour in lanthanide molecular systems is usually reached using i) chemical agents for redox reaction[18-21] and pH variation,[22-23] ii) selected solvents,[24-27] iii) light irradiation[28-31] or iv) a combination of several stimuli.[32-33] As recently reviewed,[34] lanthanides are ideal elements for the design of molecular switches since they are extremely sensitive to crystal field effects, in other words, to any structural changes in the first coordination sphere or even farther in the crystal packing. Obviously, the listed-above stimuli induced chemical modifications of the target system such as ligand or/and metal-centred oxidation state, isomerization, protonation, modification of the coordination number... leading, from a chemical point of view, to different starting and final systems. Thus, an applied pressure as external stimulus appears as a promising alternative to finely tune the SMM behaviour. The few examples of such studies have been carried out mainly on the pioneering Mn_{12} system,[35-37] as well as on other manganese-based SMMs.[38-41] To the best of our knowledge, only three examples of lanthanide complexes studied under applied pressure have been reported to date. Nevertheless, in such examples the applied pressure induced the loss of crystallinity due to the release of solvent molecules[42] or phase transition[43] and the effect of intermolecular and hyperfine interactions could not be quantitatively taken into account[44].

The mononuclear complex of formula $[Dy(tta)_3(\mathbf{L})]\cdot C_6H_{14}$ (tta^- = 2-2-thenoyltrifluoroacetonate and **L** = 4,5-bis(propylthio)-tetrathiafulvalene-2-(2-pyridyl)benzimidazole-methyl-2-pyridine) was selected from our library of compounds for high pressure studies because its magnetic properties are experimentally and computationally well-known,[45] magnetic dilutions and isotopic enrichment studies were performed[46-48] as well as spectro-electrochemistry investigations.[49] Moreover the nuclear spin free ^{162}Dy(III) (I = 0) ion was chosen to cancel the hyperfine coupling and to diminish the under-barrier magnetic relaxation mechanisms. Therefore, here we present the high-pressure single crystal X-ray diffraction study and magnetic investigations of $[^{162}Dy(tta)_3(\mathbf{L})]\cdot C_6H_{14}$ (**^{162}Dy**). The magnetic measurements are completed by those of the diluted analogue $[^{162}Dy_{0.05}Y_{0.95}(tta)_3(\mathbf{L})]\cdot C_6H_{14}$ (**^{162}Dy@Y**). Finally, periodic Density Functional Theory (DFT) and multireference wavefunction theory calculations were conducted to rationalize both structural and magnetic results.

Results and Discussion

Structural Characterization

Both **^{162}Dy** and **^{162}Dy@Y** compounds have been previously synthetized and characterized by IR and UV-visible spectroscopies, elemental analyses, and Scanning Electron Microscopy (SEM).[45,48] The structure for the natural element (**Dy**)[45], at ambient temperature, and for **^{162}Dy** and **^{162}Dy@Y**[48] at 150 K have previously been determined by single crystal X-ray diffraction.

Ambient Pressure Crystal Structure. The ambient pressure X-ray structure of **Dy** at room temperature is quickly described below. It crystallizes in the P-1 (N°2) triclinic space group. The X-ray structure revealed the formation of a mononuclear complex for which the Dy(III) centre is linked to three tta$^-$ anions and one **L** ligand through the (2-pyridyl)benzoimidazolyl (bzip) fragment (Figure 1) while a *n*-hexane solvent molecule co-crystallizes with the complex. The ligand arrangement of the resulting N_2O_6 coordination sphere led to a square antiprism with a deviation from the ideal D_{4d} symmetry of 0.54 (from SHAPE analysis).[50] The average Dy-N and Dy-O bond lengths are 2.530(5) Å and 2.333(4) Å, respectively. The location of the thiophene groups containing S31, S41, and S51 are noted in Fig. S1. The neutral form of the TTF-based ligand is confirmed by the C=C central bond length of 1.347(9) Å and boat conformation. The formation of "head-to-tail" dimers of complexes are identified in the crystal packing (Figure S2) thanks to π-π interactions between the donor (TTF fragment) and acceptor (bzip) parts of the **L** dyad.

High-Pressure Crystal Structure. The structure of **^{162}Dy** was determined at high-pressure using single crystal X-ray diffraction in the pressure range of 0.22 to 2.43 GPa (Table S1). On increasing pressure, the compression of the unit cell was found to be highly anisotropic with the *a* and *b* axes compressing more than the *c* axis (Figure S3a) with 10.3, 9.1 and 4.8 % of reduction, respectively. The angles are not strongly modified.

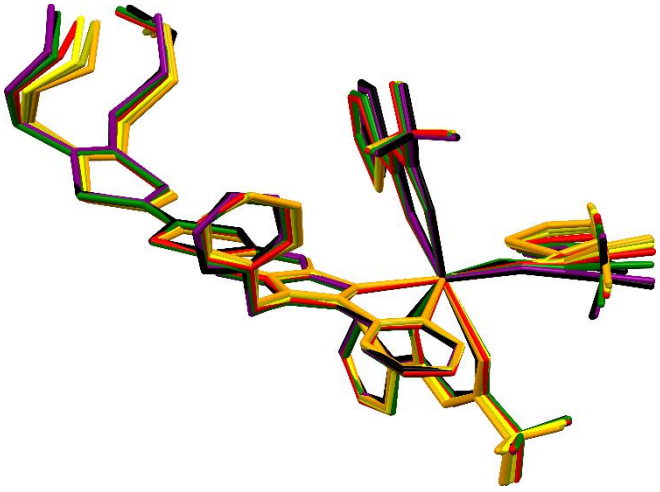

Figure 1. X-ray structure of **^{162}Dy** recorded in the pressure range 0-2.43 GPa: P = 0 GPa (black), P = 0.22 GPa (purple), P = 0.46 GPa (green), P = 1.17 GPa (red), P = 1.63 GPa (yellow), P= 2.10 GPa (yellowish) and P = 2.43 GPa (orange).

The volume of the cell decreases from 3280 Å^3 at ambient pressure to 2640 Å^3 at 2.43 GPa. To give more insights on the pressure effect on the crystal structure, a series of periodic DFT optimizations were performed at selected isostatic pressures ranging from 0 to 2.5 GPa (see Computational Details in the Experimental part). To investigate potential effects of higher pressures on the structure, two additional points were added in the study (3 and 5 GPa). The trend of the calculated cell parameters agrees with the experimental one within the 0-2.5 GPa window (Figures. S3a-c, Table S2) and validates the deformation in the [110] plane. One could identify a slight deviation between experimental and calculated trend for the γ angle at P > 1.5 GPa. Even though the effects upon the unit cell angles appear very limited, the increase of the applied pressure reduces *b* and *c* parameters reaching a minimum value at 3 GPa while *a* parameter continues to decrease. The calculations show that at 2.5 GPa, the structure almost reaches the maximal compression of the *bc* plane leaving only one degree of freedom for the dimers to shift in the cell along the *a*-axis. Further increasing the external pressure, up to 5 GPa, induces the reduction of *a* parameter down to 13.2 Å while *b* and *c* converge. The effects of increasing pressure can be seen with intramolecular distortions. The first coordination sphere of the Dy is particularly of interest. There is a reduction in the average Dy-O distances under increasing applied pressure. This average reduction was expected however the individual Dy-O are far from homogeneous. Under 2.43 GPa, Dy-O1, Dy-O4, and Dy-O6 are strongly affected respectively compressing by 2.4, 3.0, and 3.7 % of their initial length (ambient pressure). Dy-O2 (0.5 %) and Dy-O3 (0.3 %) weakly compressed while Dy-O5 is found to elongate (-1.9 %) (Figure S4, Table S3). For each ancillary ligand (tta$^-$ anions), one Dy-O bond length is compressed (Dy-O1, Dy-O4, and Dy-O6) while the second one is almost not affected (Dy- O2 and Dy-O3) or elongated (Dy-O5) under pressure. A similar trend is observed for the Dy-N distances with a strong (4.2 %) and weak (1.1 %) compression for Dy-N1 and Dy-N2, respectively (Figures. 2 and S5, Table S3).

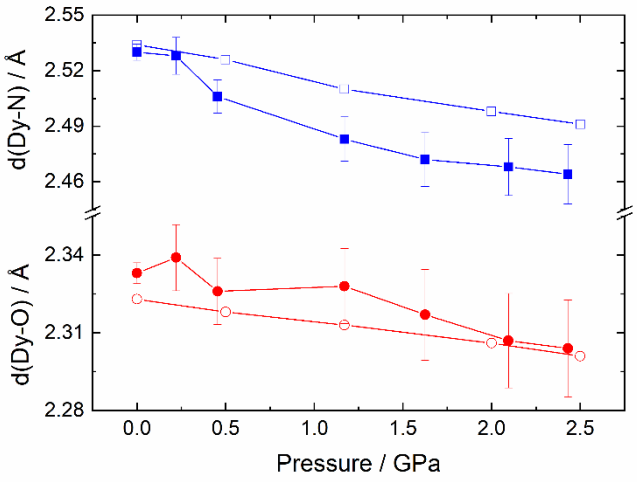

Figure 2. Experimental (full symbols) and calculated (empty symbols) variations of the average Dy-O (red) and Dy-N (blue) distances with pressure.

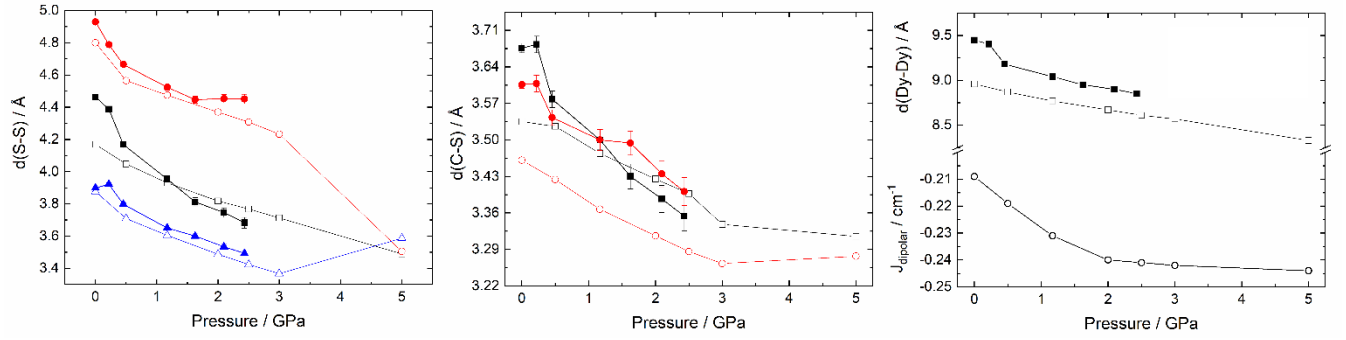

Figure 3. Pressure variations of the experimental (full symbols) and calculated (empty symbols) intramolecular distances S31···S51 (blue triangles), S31···S41 (black squares) and S41···S51 (red circles) (a), intermolecular distances C5···S4 (black squares) and C14···S2 (red circles) (b) and Dy···Dy (black squares) (c). (c) Pressure variation of the calculated antiferromagnetic dipolar interaction $J_{dipolar}$ (open black circles).

The compression trends are also observed for the Dy-O and Dy-N distances in the DFT optimized structures (Table S4). The pressure induces an increase of the Dy-X (X = O and N) bond length distribution (Figures S3 and S4) which is illustrated by the increase of the CShM(D_{4d}) coefficient (Fig. S6) determined by the SHAPE analysis.[50] Indeed the Dy-O and Dy-N distances range respectively from 2.311 to 2.347 Å and 2.496 to 2.564 Å at P = 0 GPa while at 2.43 GPa they range from 2.240 to 2.380 Å and 2.390 to 2.536 Å. The CShM(D_{4d}) increases from 0.54 to 0.65 (Fig. S6). At ambient pressure, the three thiophene groups formed only one short S31···S51 contact (3.899 Å) (Figures. 3a and S5). All the S···S intramolecular distances decrease with pressure, reaching two short S31···S51 (3.493 Å) and S31···S41 (3.683 Å) contacts (black squares, Figures 3a and S7) at the highest experimental pressure (2.43 GPa). The calculations show that at 5 GPa, the three sulphur atoms form a triangle of short S31···S51 (3.587 Å), S31···S41 (3.489 Å) and S41···S51 (3.505 Å) contacts (Figures 3a and S7). These intramolecular S···S contacts may be one of the parameters which drives the deformation of the coordination sphere around the Dy(III) centre. From an intermolecular point of view, the compression along the *b* axis is visible through the π-π distance between the two **L** ligands composing a dimer. Thus the shortest intermolecular C···S distances decrease from 3.606 (0 GPa) to 3.354 Å (2.43 GPa). The calculations show that these distances can further decrease reaching their shortest distance at 3 GPa (Figures 3b and S8) as observed for the *b* parameter (Figure S3). Finally, Fig. 3c illustrates the decrease of the intermolecular Dy···Dy distance (6.3 %) with pressure. Both computed pressure variations of the C···S and Dy···Dy intermolecular distances are in agreement with the experiment demonstrating the pertinence of the periodic DFT approach to determine the optimized structures under isostatic pressure.

Piezochromism

Single crystals of **^{162}Dy** are orange and no change of colour was observed when the crystals were ground or during the measurement of physical properties.[48] The colour is attributed to the HOMO → LUMO intra-ligand charge transfer (ILCT) centred at 23200 cm^{-1} (430 nm) where the HOMO and LUMO are respectively centred on the TTF and bzip fragments.[45] Thus the colour change can be connected to the energy of the ILCT excitation. It is also well-known that such energy can be modulated by oxidation of the TTF fragment[49] or by coordination of the electron withdrawing metal unit.[51] Figure S1 shows that a single crystal of **^{162}Dy** changes of colour from orange to purple when applying an external pressure from 0.22 GPa to 2.43 GPa. This piezochromic phenomena could be explained by pressure perturbation to the LUMO energy level of the related ILCT transition because of the shortening of the Dy-N1 bond length which increase the electrostatic effect of the $Dy(tta)_3$ coordination. Piezochromism is reversible since the single crystal recovers its initial colour releasing the cell pressure (see video in SI).

Magnetism

The thermal dependence of the $\chi_M T$ at P = 0 GPa, 0.31 GPa, 1.17 GPa and back to 0 GPa are depicted in Figure S9. The measurements are limited to the 5-100 K temperature range due to the used setup. No significant effect of the pressure could be observed on the $\chi_M T(T)$ curves on such temperature range. The frequency dependences of the magnetic susceptibility (χ_M) have been measured to determine the dynamic magnetic properties of **^{162}Dy** at ambient pressure (0 GPa) and high pressure (0.31 and 1.17 GPa). It is worth noting that the dynamic magnetic properties of **^{162}Dy** at ambient pressure are already well-known[48] but the measurements were repeated using the same squid magnetometer and set up as the high-pressure magnetic measurements. At P = 0 GPa, **^{162}Dy** displays frequency dependence of the magnetic susceptibility (Figures 4a and S10a), the appearance of an out-of-phase component (χ_M") in zero applied magnetic field is sign of slow magnetic relaxation. At 2 K, the maximum on the χ_M" vs. ν curve (where ν is the frequency of the oscillating field) is centred at 15 Hz (Figure 4a) in agreement with the published frequency value[48] highlighting that the pressure cell has no significant influence. Increasing the applied pressure, the slow magnetic relaxation is preserved but shifts to higher frequencies with maxima at 2 K centred at 20 Hz for 0.31 GPa (Figure 4b) and 50 Hz (Fig. 4c) for 1.17 GPa. The effect of the pressure is reversible since the release of the pressure allowed the recovery of the initial ac data (Figure 4d) and that is in line with the reversible piezochromic effect.

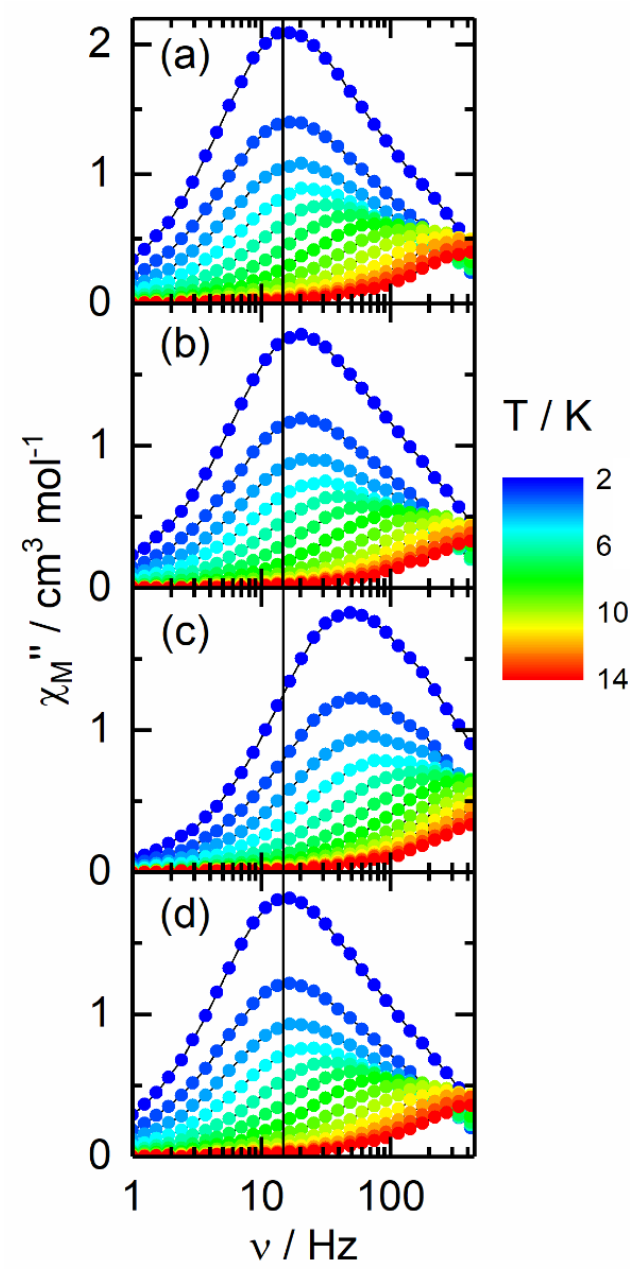

Figure 4. Frequency dependence of χ_M" in the temperature range 2-14 K for **^{162}Dy** under P = 0 GPa (a), P = 0.31 GPa (b), P = 1.17 GPa (c) and back to P = 0 GPa (d) in zero applied magnetic field. The full vertical line is guide to the eye only.

The relaxation time τ was extracted at each temperature and applied pressure using an extended Debye model (details in SI, Table S5) to fit simultaneously the frequency dependence of χ_M'' and of the in-phase susceptibility χ_M' (Figure S11). Figures S12-S15 show the normalized Cole-Cole plots in the temperature range of 2 to 14 K. Whatever the pressure, the resulting plots adopt a semi-circle shape giving a narrow distribution of the relaxation times (0.01<α<0.15) (Tables S5-S8). The relaxation time follows a combination of thermally dependent and thermally independent processes (Figure 5).

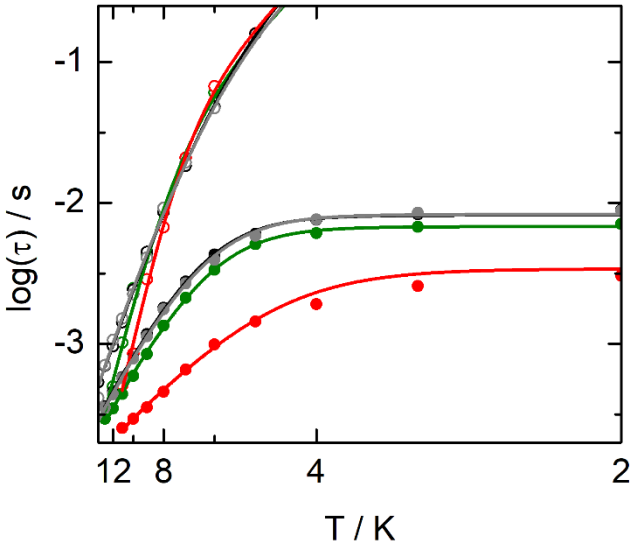

Figure 5. Arrhenius plots of the relaxation time in zero applied magnetic field (full symbols) and at 1000 Oe (empty symbols) for **^{162}Dy** at P = 0 GPa (black), P = 0.31 GPa (green), P = 1.17 GPa (red) and back to P = 0 GPa (gray). Full lines are the best-fitted curves (see text). The relaxation time at 5 K under 1000 Oe was manually extracted.

Until the present work, the Arrhenius law of the ^{x}**Dy** (x = 161 to 164) systems in its natural and its isotopically enriched form was fitted using a combination of Orbach and QTM process and neglecting the Raman process[47] (equation 1):

$$\tau^{-1} = \underbrace{CT^n}_{Raman} + \underbrace{\tau_0^{-1}\exp\left(-\frac{\Delta}{kT}\right)}_{Orbach} + \underbrace{\tau_{TI}^{-1}}_{QTM} \qquad \text{Eq. 1}$$

Using such an approach, the best fits of the thermal dependence of the relaxation time in the pressure range of 0-1.17 GPa in zero applied magnetic field are shown in Figure S16 with the parameters in Table S9.

The ac magnetic properties were studied under an applied optimal magnetic field of 1000 Oe in the pressure range 0-1.17 GPa (Figures S17 and S18). The magnetic field cancels the fast magnetic relaxation through Quantum Tunnelling of the Magnetization (QTM) and thus the maxima of the χ_M" are shifted to the lower frequencies. The same method than for zero magnetic field was used to extract the relaxation time τ at 1000 Oe (Tables S10-13). The distribution of the relaxation times increases (0.01<α<0.40) due to the dc applied magnetic field (Figures S19-22). Under the 1000 Oe optimal field, the relaxation time follows thermally dependent processes with a deviation from the linearity at low temperature which has been attributed to the Raman contribution (Figure 5, equation 1). Thus, the thermal dependence of the relaxation time at P = 0 GPa and H = 1000 Oe was fitted using a combination of Orbach and Raman processes. The best fit was obtained for an Orbach regime with Δ = 53(3) K, τ_0 = 1.7(8)×10^{-5} s and Raman regime C = 2.4(2)×10^{-3} s^{-1} K^{-n}, n = 4.76(56) between 5 and 14 K. The expected n value for Kramers ions should be 9,[52] but the presence of both acoustic and optical phonons could lead to lower values comprised between 2 and 7.[53-56]

Table 1. Dynamic parameters of the different relaxation mechanisms for the **^{162}Dy** in the pressure range of 0-1.17 GPa

P / GPa	H / kOe	Δ / K	τ_0 / s	C / K^{-n} s^{-1}	n	τ_{TI} / s
0	0	34.7(7)	$3.2(3)\times10^{-5}$	0.0025(2)	4.76	0.0082
0	1	54(1)	$1.6(2)\times10^{-5}$			-
0.31	0	34(1)	$2.6(5)\times10^{-5}$	0.0032(2)	4.76	0.0068
0.31	1	82(4)	$8(3)\times10^{-5}$			-
1.17	0	21(4)	$4.4(8)\times10^{-5}$	0.0028(2)	4.76	0.0034
1.17	1	90(5)	$1.5(7)\times10^{-5}$			-
Back to 0	0	34(1)	$3.4(5)\times10^{-5}$	0.0029(6)	4.76	0.0083
Back to 0	1	55(3)	$1.7(3)\times10^{-5}$			-

In order to prevent any over parametrization, all the next fits have been realized with fixed *n* = 4.76 and the QTM fixed to the values found using a combination of Orbach and QTM processes only (Table S9). The Raman process is considered field independent (equation 1)[57] for a given pressure but variable as a function of the applied pressure since such stimulus induced reorganization of the electronic distribution around the Dy(III) centre and variation of the interaction between the complex and the matrix. Then, the thermal variation of the relaxation time at a specific pressure is simultaneously fitted for **^{162}Dy** under 0 Oe and 1000 Oe with contribution of two effective Orbach processes, Raman shared parameters and zero-field only QTM. The best fits for P = 0 GPa (Figure S23), P = 0.31 GPa (Figure S24), 1.17 GPa (Figure S25) and back to P = 0 GPa (Figure S26) are given in the Table 1 and displayed in Figure 5. From the data of Table 1 and Figure S27, one could remark that i) the energy barrier values increased under applied magnetic field for a given pressure due to the reduction of ground-state QTM,[58] ii) in zero magnetic field, the increase of applied pressure led to a decrease of the fitted energy barrier and an increase of the QTM which could be related to the distortion of the coordination sphere around the Dy(III) centre (Figure S6) and iii) the pressure effect on the dynamic magnetic properties is reversible. Nevertheless, no significant variation of the Raman process (CT^n) was observed (Table 1). This could be due to the available data limited to the experimental temperature range of 5-12 K because the system displays too slow magnetic relaxation at lower temperature for our setup. Thus, lower temperature dc measurements could give more insights on this point.

The classical butterfly shape hysteresis loops for **^{162}Dy** was measured at 2 K and P = 0 GPa then compared to those under applied pressure (Figure 6). While all the hysteresis loops remain close at zero field due to the QTM, significant differences are observed in field. Application of high-pressure tends to close the hysteresis loop in field (δ = 650 0e at H = 1000 Oe for P = 0 GPa and (δ = 400 0e at H = 1000 Oe for P = 1.17 GPa) (Figure S28) in agreement with the increase of the under energy barrier mechanisms (QTM and Raman). The previous magnetic investigation in frozen solution of **Dy**[44] and for diluted **^{162}Dy**[48] undoubtedly demonstrated the presence of significant intermolecular dipolar interactions playing a drastic role in the magnetic behaviour.

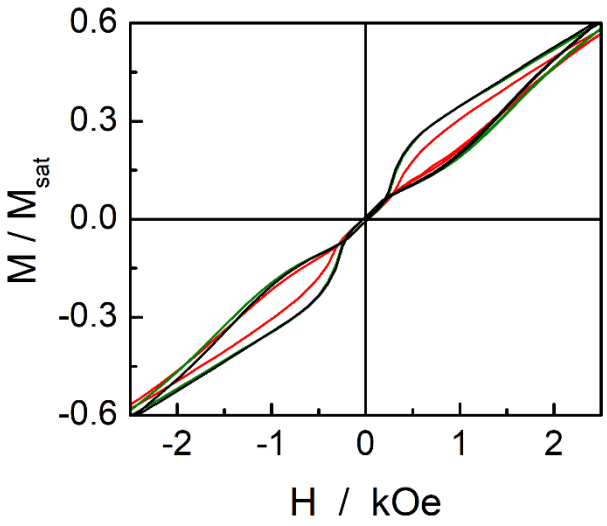

Figure 6. Magnetic hysteresis loops at 2 K and at a sweep rate of 16 Oe s^{-1} for **^{162}Dy** at 0 GPa (black), 0.31 GPa (green) and 1.17 GPa (red).

Thus, to discriminate between an intra- and/or inter-molecular origin of the magnetic modulation under applied pressure, the magnetic study was carried out for the diluted **^{162}Dy@Y** compound. The constraints due to the small volume of the setup and the weak magnetic response of **^{162}Dy@Y** limited the magnetic study to the dc investigation. The butterfly shape hysteresis loops is also observed for **^{162}Dy@Y** at 2 K and P = 0 GPa (Figure S29). A magnetic memory is observed at smaller applied magnetic field for **^{162}Dy@Y** than for **^{162}Dy** due to the decrease of QTM by magnetic dilution. The variation of the hysteresis opening is not homogenous in increasing the applied pressure. Indeed, the opening at 600 Oe first increases from δ = 450 Oe at 0 GPa to δ = 590 Oe at 0.55 GPa and then decreases to δ = 520 Oe at 1.04 GPa (Figure 7).

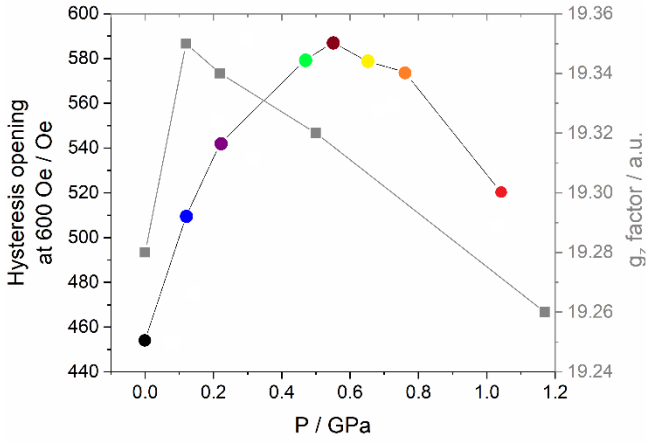

Figure 7. Hysteresis loop opening at H = 600 Oe and g_z factor values (gray full squares) in the pressure range of 0-1.04 GPa. Full lines are guides to the eye only.

The variation of the hysteresis loop width of **^{162}Dy@Y** is mainly representative of the intramolecular structural modification induced by the pressure. The magnetic modulation at a given applied field and the butterfly hysteresis shape could not be attributed to QTM since both hyperfine and dipolar interactions have been cancelled and might be due to the Raman process. From the DC magnetic investigations of **^{162}Dy** and **^{162}Dy@Y**, it appeared that the magnetic modulation under applied pressure are different leading to the involvement of both intra- and inter-molecular origins. It can be anticipated that wavefunction theory calculations could rationalize this magnetic behaviour.

Ab Initio Calculations

SA-CASSCF/RASSI-SO calculations were performed to propose a quantitative interpretation of the magnetic data. Such wavefunction calculations were carried out from the crystal structure of **Dy** at room temperature. In order to go one step forward compared to the calculations previously performed by some of us using an isolated complex ("gas phase"),[45] the structural model was optimized taking into account the neighbouring complexes ("solid state") using periodic DFT calculations (Figure S30). Based on the latter optimized structure, the ground state doublet (GS) for the single ion at P = 0 GPa has a slightly less Ising character (g_x = 0.02, g_y = 0.03 and g_z = 19.28, Table 2) than the GS obtained with the isolated complex (g_x = 0.00, g_y = 0.00 and g_z = 19.50, Table S14). The ground state doublet is mainly composed of $M_J = \pm 15/2$ (91%) and the orientation of the main anisotropy axis is calculated perpendicular to the plane involving the bzip fragment as expected for an oblate Dy(III) ion in a N_2O_6 coordination sphere (Figure S31).[58-63] The energy gap between the GS and the first excited state decreases from 125.7 cm^{-1} to 98.8 cm^{-1} (Figure S30 and Table S14). The calculated energy barrier of 98.8 cm^{-1} is higher than the effective energy barrier determined from the high temperature region of the Arrhenius plot at 0 Oe (23.6(2) cm^{-1}) and 1000 Oe (50.3(7) cm^{-1}) supporting the presence of significant under barrier magnetic relaxation mechanisms such as QTM and Raman.

Table 2. Energy gap between the ground state (GS) and first excited state (ΔE) of the $^6H_{15/2}$ multiplet with composition of GS and g factor values at selected applied pressure.

P/GPa	g_x	g_y	g_z	GS	ΔE (cm^{-1})
0	0.02	0.03	19.28	90.6% ± 15/2	98.8
0.12	0.02	0.03	19.35	92.0% ± 15/2	103.0
0.22	0.02	0.03	19.34	91.0% ± 15/2	100.0
0.5	0.02	0.03	19.32	91.1% ± 15/2	96.6
1.17	0.04	0.06	19.26	90.4% ± 15/2	80.0
2	0.06	0.12	19.15	89.0% ± 15/2	63.2
2.5	0.10	0.23	18.99	87.9% ± 15/2	49.3
3	0.13	0.37	18.87	87.2% ± 15/2	40.2
5	0.05	0.31	18.94	87.1% ± 15/2	48.2

Calculations show that by applying weak pressure (P < 0.5 GPa), the uniaxial character of the GS magnetic anisotropy is enhanced (Table 2) while for higher pressure values, the transversal components of the g factor increase leading to more efficient QTM (Tables S15-S23). This trend perfectly agreed with what was observed with the hysteresis loop of **^{162}Dy@Y**. One more important parameter is the decrease of the energy barrier for applied pressures P > 0.5 GPa as experimentally observed (Table 1). The matrix elements of the transition magnetic moments have been computed and depicted in Figure S32 in order to give more insights into the relaxation mechanisms. Thus the increase of applied pressure induced a decrease of the spin-phonon Orbach process (1.57 for 0 GPa to 0.90 for 2.0 GPa) in favour to both under barrier Raman (0.11 for 0 GPa to 0.57 for 3.0 GPa) and (0.02 for 0 GPa to 0.08 for 3.0 GPa) QTM processes (Figure S30). The hysteresis loops of both **^{162}Dy** and **^{162}Dy@Y** compounds suggested a significant role of the intermolecular interaction (J_{dip}), the latter were computed and evaluated to J_{dip} = -0.209 cm^{-1} at P = 0 GPa. Increasing the pressure, the absolute J_{dip} value increases to 0.244 cm^{-1} (Figure 3c) in agreement with the shortening of the intermolecular Dy···Dy distances (Figure 3c) and tends to reinforce the QTM.

Conclusion

In conclusion, this work demonstrated the possibility to reversibly modulate the SMM behaviour of a mononuclear complex of Dy(III) applying pressure. The stimulus induced weak structural distortions at the molecular level at the origin of the change in the electronic properties. The combined magnetic investigations of **^{162}Dy** and **^{162}Dy@Y** under applied pressure demonstrated that the degradation of the slow magnetic relaxation performances might be due to the decrease of the Orbach contribution in favour of the under-barrier Raman and QTM contributions. The pressure-magnetic modulation is mainly due to intermolecular origin (dipolar interactions and interaction with the matrix) with a weak contribution of the intramolecular origin (distortion of the coordination sphere around the metal centre). This work reports a combination of reversible piezochromism and pressure-magnetic modulation of the SMM behaviour. The **^{162}Dy** compound enriches the family of multiple properties SMM and could open the route to the design of optical and magnetic molecular sensors.

Experimental Section

Materials and Methods. The compounds $[^{162}Dy(tta)_3(\mathbf{L})]\cdot C_6H_{14}$ (**^{162}Dy**) and its diluted analogue $[^{162}Dy_{0.05}Y_{0.95}(tta)_3(\mathbf{L})]\cdot C_6H_{14}$ (**^{162}Dy@Y**) (tta^- = 2-thenoyltrifluoroacetylacetonate anion and **L** = 4,5-bis(propylthio)-tetrathiafulvalene-2-(2-pyridyl)benzimidazole-methyl-2-pyridine) were synthesized following previously reported method.[48] All solvents were dried using standard procedures. The isotopically enriched $^{162}Dy_2O_3$ oxides are commercially available from Eurisotop and Innovachem companies. All other reagents were purchased from Merck Co. Ltd and were used without further purification.

Single-crystal X-ray diffraction. High-pressure experiments on **^{162}Dy** were performed using a modified Merrill-Bassett diamond anvil cell (DAC). A single-crystal was loaded into a stainless-steel gasket with ruby in the DAC to measure the pressure The pressure was measured before and after data collection and an average used. Fluorinert FC-70 was used as a pressure transmitting medium. These data were collected at room temperature on a Bruker D8 Vantage at Newcastle University equipped with a Incoatec Ag IμsK α (λ = 0.56086 Å) source and Photon II detector. Data were collected, using 10 phi scans to maximize accessible coverage. Sample reflections were identified using the reciprocal lattice viewer within the Apex II program[64] for initial unit cell refinement. Data integration and global cell refinement were performed with the program SAINT[65] and data were corrected for absorption with the program SADABS.[66] The minimum transmission factor for the high-pressure structures is due to partial shadowing from the DAC gasket. Structural solutions and least-squares refinements were carried out using the Olex2 interface to the SHELX[67][68] suite of programs. Suitable structures were obtained for six pressures: 0.22 GPa, 0.46 GPa, 1.17 GPa, 1.63 GPa, 2.10 GPa and 2.43 GPa. Complete crystal structure results as CIF files including bond lengths, angles, and atomic coordinates are deposited as Supporting Information. They have been deposited in the Cambridge Structural Data Centre and Fachinformationszentrum Karlsruhe Access Structures service (www.ccdc.cam.ac.uk/Structures) for **^{162}Dy** at P = 0.22 GPa (CCDC2154808), 0.46 GPa (CCDC2154806), 1.17 GPa (CCDC2154807), 1.63 GPa (CCDC2154805), 2.10 GPa (CCDC2154804) and 2.43 GPa (CCDC2154809), respectively.

Magnetic measurements. Magnetic measurements under pressure were performed using Quantum Design MPMS3 SQUID magnetometer equipped with a 7 T magnet. Polycrystalline samples of 11.5 mg for **^{162}Dy** and 11.4 mg for **^{162}Dy@Y** were loaded into the CuBe piston-cylinder type high pressure capsule cell (HMD, Japan) and Daphne 7373 oil was used as a pressure-transmitting medium. The actual pressure in the pressure cell was determined with approximately 0.02 GPa accuracy from the linear pressure dependence of the superconducting transition of high-purity lead (dT_c/dp = 0.379 K/GPa). The residual field of the superconducting magnet was cancelled before each measurement using the magnet reset option. The magnetic data for both compounds were corrected for the diamagnetic contribution as calculated with Pascal's constants. The in-phase and out-of-phase AC signal collected in the 1-500 Hz range at 25 K was subtracted from the corresponding data recorded between 2 and 14 K leading to the clean χ' and χ'' signals of the sample. Generally, the AC magnetic measurements in metallic sample holders such as CuBe (conductors) appear to be unusable due to the significant background related to eddy currents (loops of electric current). The eddy currents lead to the in-phase and out-of-phase AC signal of the pressure cell body that are frequency dependent and much stronger than the AC magnetic susceptibility of the sample itself (Figure S33). We have noticed, however, that the AC signal of the pressure cell body is temperature independent, and used this observation to extract the magnetic signal of the sample. This works well for data up to 500 Hz, however, at frequencies >500 Hz the AC signal becomes too distorted as the eddy currents become too strong.

Computational details. Periodic DFT calculations enhanced by dispersion correction using the D3 method[69] were carried using the VASP code (version 5.4)[70]-[72] within the GGA approximation. The functional of Perdew,Bruke and Ernzerhof (PBE)[73] was used with a plane-wave basis set defined by an energy cut-off of 450 eV and the Projector Augmented Wave (PAW) atomic pseudopotentials.[74][75] The standard PAW potentials were used for the C, F, H, S, N and O atoms while the Dy_3 pseudopotential was used to describe the Dy atoms. The calculations were carried on the Γ-point only (adding more k-points would be too time consuming due to the large size of the unit cell). The effects of the hydrostatic pressure were enforced by the stress tensor through the PSTRESS keyword. A series of selected pressures (0, 0.12, 0.22, 0.5, 1.17, 2, 2.5, 3 and 5GPa) were used to mimic the experimental conditions and to go beyond the experimental limitations. Wavefunction-based calculations were carried out on the optimized molecular structures at every selected pressure by using the SA-CASSCF/RASSI-SO approach, as implemented in the MOLCAS quantum chemistry package (versions 8.0).[76] In this approach, the relativistic effects are treated in two steps on the basis of the Douglas–Kroll Hamiltonian. First, the scalar terms were included in the basis-set generation and were used to determine the spin-free wavefunctions and energies in the complete active space self-consistent field (CASSCF) method.[77] Next, spin-orbit coupling was added within the restricted-active-space state-interaction (RASSI-SO) method, which uses the spin-free wavefunctions as basis states.[78][79] The resulting wavefunctions and energies are used to compute the magnetic properties and g-tensors of the lowest states from the energy spectrum by using the pseudospin S = 1/2 formalism in the SINGLE_ANISO routine.[80],[81] Cholesky decomposition of the bielectronic integrals was employed to save disk space and speed-up the calculations.[82] The active space of the self-consistent field (CASSCF) method consisted of the nine 4f electrons of the Dy(III) ion spanning the seven 4f orbitals, i.e. CAS(9,7)SCF. State-averaged CASSCF calculations were performed for all of the sextets (21 roots), all of the quadruplets (224 roots), and 300 out of the 490 doublets (due to software limitations) of the Dy(III) ion. 21 sextets, 128 quadruplets, and 107 doublets were mixed through spin−orbit coupling in RASSI-SO. All atoms were described by ANO-RCC basis sets.[83]-[85] The following contractions were used: [8s7p4d3f2g1h] for Dy atoms, [4s3p2d] for O and N atoms, [3s2p] for C atoms, [4s3p] for S atoms and [2s] for H atoms.

The dipole-dipole interaction between two magnetic centers 1 and 2, bearing the magnetic moment μ_1 and μ_2 respectively, is described as

$$H_{dip} = -\frac{1}{R_{12}^3}\,\mu_1 \cdot \mu_2 - 3(\mu_1 \cdot \vec{r}_{12})(\mu_2 \cdot \vec{r}_{12})$$

where R_{12} corresponds to the distance between the magnetic centers and $\vec{r}_{12}$ stands for the unit vector along the 12 direction. The resulting dipolar coupling J_{dip} constants were computed between the two closest Dy(III) monomers.

Acknowledgements

This work was supported by the CNRS, Université de Rennes 1 and the European Commission through the ERC-CoG 725184 MULTIPROSMM (project n. 725184). B.L.G. and V.M. thank the French GENCI/IDRIS-CINES centres for high-performance computing resources.

Keywords: Tetrathiafulvalene • Dysprosium • Isotopes • Single-Molecule Magnet • Pressure

[1] R. Sessoli, H. L. Tsai, A. R. Schake, S. Y. Wang, J. B. Vincent, K. Folting, D. Gatteschi, G. Christou, D. N. Hendrickson, *J. Am. Chem. Soc.* **1993**, *115*, 1804-1816.

[2] R. Sessoli, D. Gatteschi and A. Caneschi, M. A. Novak, *Nature* **1993**, *365*, 141-143.

[3] N. Ishikawa, M. Sugita, T. Ishikawa, S. Koshihara, Y. Kaizu, *J. Am. Chem. Soc.* **2003**, *125*, 8694-8695.

[4] R. Sessoli, A. K. Powell, *Coord. Chem.Rev.* **2009**, *253*, 2328–2341.

[5] D. N. Woodruff, R. E. P. Winpenny, R. A. Layfield, *Chem. Rev.* **2013**, *113*, 5110–5148.

[6] F. Pointillart, O. Cador, B. Le Guennic, L. Ouahab, *Coord. Chem. Rev.* **2017**, *346*, 150–175.

[7] Z. Zhu, M. Guo, X.-L. Li, J. Tang, *Coord. Chem. Rev.* **2019**, *378*, 350-364.

[8] C. A. Gould, K. R. McClain, D. Reta, J. G. C. Kragskow, D. A. Marchiori, E. Lachman, E.-S. Choi, J. G. Analytis, R. D. Britt, N. F. Chilton, B. G. Harvey, J. R. Long, *Science* **2022**, *375*, 198-202.

[9] N. F. Chilton, *Inorg. Chem.* **2015**, *54*, 2097-2099.

[10] L. Ungur, L. F. Chibotaru, *Chem. Eur. J.* **2017**, *23*, 3708-3718.

[11] F.-S. Guo, B.-M. Day, Y.-C. Chen, M.-L. Tong, A. Mansikkamäki, R. A. Layfield*, Angew. Chem., Int. Ed*. **2017**, *56*, 11445-11449.

[12] C. A. P. Goodwin, F. Ortu, D. Reta, N. F. Chilton, D. Mills, *Nature* **2017**, *548*, 439-442.

[13] K. R. McClain, C. A. Gould, K. Chakarawet, S. J. Teat, T. J. Groshens, J. R. Long and B. G. Harvey, *Chem. Sci.* **2018**, *9*, 8492-8503.

[14] F.-S. Guo, B.-M. Day, Y.-C. Chen, M.-L. Tong, A. Mansikkamäki, R. A. Layfield, *Science* **2018**, 362, 1400-1403.

[15] S. Thiele, F. Balestro, R. Ballou, S. Klyatskaya, M. Ruben, W. Wernsdorfer, *Science* **2014**, *344*, 1135-1138.

[16] K. S. Pedersen, A.-M. Ariciu, S. McAdams, H. Weihe, J. Bendix, F. Tuna, S. Piligkos, *J. Am. Chem. Soc.* **2016**, *138*, 5801-5804.

[17] O. Sato, *Nat. Chem.* **2016**, *8*, 644-656.

[18] P. Zhang, M. Perfetti, M. Kern, P. P. Hallmen, L. Ungur, S. Lenz, M. R. Ringenberg, W. Frey, H. Stoll, G. Rauhut, J. van Slageren, *Chem. Sci.* **2018**, *9*, 1221–1230.

[19] B. S. Dolinar, S. Gomez-Coca, D. I. Alexandropoulos, K. R. Dunbar, *Chem. Commun.* **2017**, *53*, 2283–2286.

[20] M. Gonidec, E. S. Davies, J. McMaster, D. B. Amabinino, J. Veciana, *J. Am. Chem. Soc.* **2010**, *132*, 1756–1757.

[21] C. M. Dickie, A. L. Laughlin, J. D. Wofford, N. S. Bhuvanesh, M. Nippe, *Chem. Sci.* **2017**, *8*, 8039–8049.

[22] D. Tanaka, T. Inose, H. Tanaha, S. Lee, N. Ishikawa, T. Ogawa, *Chem. Commun.* **2012**, *48*, 7796–7798.

[23] Z. Liang, M. Damjanovic, M. Kamila, G. Cosquer, B. K. Breedlove, M. Enders, M. Yamashita, *Inorg. Chem.* **2017**, *56*, 6512–6521.

[24] K. Suzuki, R. Sato, N. Mizuno, *Chem. Sci.* **2013**, *4*, 596–600.

[25] J.-L. Liu, Y.-C. Chen, Y.-Z. Zheng, W.-Q. Lin, L. Ungur, W. Wernsdorfer, L. F. Chibotaru, M.-L. Tong, *Chem. Sci.* **2013**, *4*, 3310–3316.

[26] X. Zhang, V. Vieru, X. Feng, J.-L. Liu, Z. Zhang, B. Na, W. Shi, B.-W. Wag, A. K. Powell, L. F. Chibotaru, S. Gao, P. Cheng, J. R. Long, *Angew. Chem., Int. Ed.* **2015**, *54*, 9861–9865.

[27] J.-Y. Ge, L. Cui, J. Li, F. Yu, Y. Song, Y.-Q. Zhang, J.-L. Zuo, M. Kurmoo, *Inorg. Chem.* **2017**, *56*, 336–343.

[28] D. Pinkowicz, M. Ren, L.-M. Zheng, S. Sato, M. Hasegawa, M. Morimoto, M. Irie, B. K. Breedlove, G. Cosquer, K. Katoh, M. Yamashita, *Chem.–Eur. J.* **2014**, *20*, 12502–11513.

[29] L.-F. Wang, J.-Z. Qiu, J.-L. Liu, Y.-C. Chen, J.-H. Jia, J. Jover, E. Ruiz, M.-L. Tong, *Chem. Commun.* **2015**, *51*, 15358–15361.

[30] P. Selvanathan, V. Dorcet, T. Roisnel, K. Bernot, G. Huang, B. Le Guennic, L. Norel, S. Rigaut, *Dalton Trans.* **2018**, *47*, 4139–4148.

[31] M. Hojorat, H. Al Sabea, L. Norel, K. Bernot, T. Roisnel, F. Gendron, B. Le Guennic, E. Trzop, E. Collet, J. R. Long, S. Rigaut, *J. Am. Chem. Soc.* **2020**, *142*, 931-936.

[32] H. Tian, J.-B. Su, S.-S. Bao, M. Kurmoo, X.-D. Huang, Y.-Q. Zhang, L.-M. Zheng, *Chem. Sci.* **2018**, *9*, 6424–6433.

[33] F. Pointillart, J. Flores Gonzalez, V. Montigaud, L. Tesi, V. Cherkasov, B. Le Guennic, O. Cador, L. Ouahab, R. Sessoli, V. Kuropatov, *Inorg. Chem. Front.* **2020**, *7*, 2322-2334.

[34] O. Cador, B. Le Guennic, F. Pointillart, *Inorg. Chem. Front.* **2019**, *6*, 3398-3417.

[35] Y. Suzuki, Y. Takeda, K. Awaga, *Phys. Rev. B* **2003**, *67*, 132402.

[36] A. Sieber, R. Bircher, O. Waldmann, G. Carver, G. Chaboussant, H. Mutka, H.-U. Güdel, *Angew. Chem., Int. Ed.* **2005**, *44*, 4239-4242.

[37] R. Bircher, G. Chaboussant, C. Dobe, H.-U. Güdel, S. T. Ochsenbein, A. Sieber, O. Waldmann, *Adv. Funct. Mater.* **2006**, *16*, 209-220.

[38] A. Sieber, G. Chaboussant, R. Bircher, C. Boskovic and H.-U. Güdel, *Phys. Rev. B* **2004**, *70*, 172413.

[39] A. Prescimone, C. J. Milios, S. Moggach, J. E. Warren, A. R. Lennie, J. Sanchez-Benitez, K. Kamenev, R. Bircher, M. Murrie, S. Parsons, E. K. Brechin, *Angew. Chem., Int. Ed.* **2008**, *47*, 2828-2831.

[40] A. Prescimone, C. J. Milios, J. Sanchez-Benitez, K. V. Kamenev, C. Loose, J. Kortus, S. Moggach, M. Murrie, J. E. Warren, A. R. Lennie, S. Parsons, E. K. Brechin, *Dalton Trans.* **2009**, 4858-4867.

[41] A. Prescimone, J. Sanchez-Benitez, K. V. Kamenev, S. A. Moggach, A. R. Lennie, J. E. Warren, M. Murrie, S. Parsons, E. K. Brechin, *Dalton Trans.* **2009**, 7390-7395.

[42] W.-B. Chen, Y.-C. Chen, J.-L. Liu, J.-H. Jia, L.-F. Wang, Q.-W. Li, M.-L. Tong, *Inorg. Chem.* **2017**, *56*, 8730-8734.

[43] M. S. Norre, C. Gao, S. Dey, S. K. Gupta, A. Borah, R. Murugavel, G. Rajaraman, J. Overgaard, *Inorg. Chem.* **2020**, *59*, 717-729.

[44] V. S. Parmar, A. M. Thiel, R. Nabi, G. K. Gransbury, M. S. Norre, P. Evans, S. C. Corner, J. M. Skelton, N. F. Chilton, D. P. Mills, J. Overgaard, *Chem. Commun.* DOI: 10.1039/D2CC06722F.

[45] T. T. da Cunha, J. Jung, M.-E. Boulon, G. Campo, F. Pointillart, C. L. M. Pereira, B. Le Guennic, O. Cador, K. Bernot, F. Pineider, S. Golhen, L. Ouahab, *J. Am. Soc. Chem.* **2013**, *135*, 16332-16335.

[46] F. Pointillart, K. Bernot, S. Golhen, B. Le Guennic, T. Guizouarn, L. Ouahab, O. Cador, *Angew. Chem., Int. Ed.* **2015**, *54*, 1504-1507.

[47] L. Tesi, Z. Salman, E. Cimatti, F. Pointillart, K. Bernot, M. Mannini, R. Sessoli, *Chem. Commun.* **2018**, *54*, 7826-7829.

[48] J. Flores Gonzalez, F. Pointillart, O. Cador, *Inorg. Chem. Front.* **2019**, *6*, 1081-1086.

[49] G. Fernandez Garcia, V. Montigaud, L. Norel, O. Cador, B. Le Guennic, F. Totti, F. Pointillart, *Magnetochemistry* **2019**, *5*, 46-60.

[50] M. Llunell, D. Casanova, J. Cirera, P. Alemany and S. Alvarez, S. *SHAPE Program for the Stereochemical Analysis of Molecular Fragments by Means of Continuous Shape Measures and Associated Tools;* Departament de Quimica Fisica, Departament de Quimica Inorganica and Institut de Quimica Teorica i Computacional-Universitat de` Barcelona: Barcelona, Spain.

[51] F. Pointillart, T. Cauchy, O. Maury, Y. Le Gal, S. Golhen, O. Cador, L. Ouahab, *Chem. Eur. J.* **2010**, *16*, 11926-11941.

[52] A. Abragam, B. Bleaney, Electron Paramagnetic Resonance of Transition Ions, Clarendon Press, Oxford, **1970**.

[53] A. Singh, K. N. Shrivastava, *Phys. Status Solidi B* **1979**, *95*, 273–277.

[54] K. N. Shrivastava, *Phys. Status Solidi B* **1983**, *177*, 437–458.

[55] C. A. P. Goodwin, D. Reta, F. Ortu, N. F. Chilton, D. P. Mills, *J. Am. Chem. Soc*. **2017**, *139*, 18714−18724.

[56] L. Gu, R. Wu, *Phys. Rev. B* **2021**, *103*, 014401.

[57] R. Orbach, *Proc. R. Soc. London, Ser. A* **1961**, *264*, 458–484.

[58] D. Errulat, B. Gabidullin, A. Mansikkamaki, M. Murugesu, *Chem. Commun*. **2020**, *56*, 5937-5940.

[59] F. Pointillart, J. Jung, R. Berraud-Pache, B. Le Guennic, V. Dorcet, S. Golhen, O. Cador, O. Maury, Y. Guyot, S. Decurtins, S.-X. Liu, L. Ouahab, *Inorg. Chem.* **2015**, *54*, 5384-5397

[60] J.-K. Ou-Yang, N. Saleh, G. Fernandez Garcia, L. Norel, F. Pointillart, T. Guizouarn, O. Cador, F. Totti, L. Ouahab, J. Crassous, B. Le Guennic, *Chem. Commun*. **2016**, *52*, 14474-14477.

[61] B. Lefeuvre, O. Galangau, J. Flores Gonzalez, V. Montigaud, V. Dorcet, L. Ouahab, B. Le Guennic, O. Cador, F. Pointillart, *Front. Chem.* **2018**, *6*, 552-562.

[62] F. Pointillart, J. -K. Ou-Yang, G. Fernandez Garcia, V. Montigaud, J. Flores Gonzalez, R. Marchal, L. Favereau, F. Totti, J. Crassous, O. Cador, L. Ouahab, B. Le Guennic, *Inorg. Chem.* **2019**, *58*, 52-56.

[63] O. Galangau, J. Flores Gonzalez, V. Montigaud, V. Dorcet, B. Le Guennic, O. Cador and F. Pointillart, Magnetochemistry, 2020, 6, 19-33.

[64] Sheldrick, G. M. Bruker Apex II; Bruker AXS Inc.: Madison, WI, **2004**.

[65] SAINT; Bruker AXS Inc.: Madison, WI, **2007**.

[66] SADABS; Bruker AXS Inc., Madison, WI, **2001**.

[67] G. M. Sheldrick, *Acta Crystallogr., Sect. C: Struct. Chem.,* 2015, **71**, 3−8.

[68] G. M. Sheldrick, *Acta Crystallogr., Sect. A: Found. Crystallogr.,* 2008, **64**, 112−122.

[69] S. Grimme, J. Antony, S. Ehrlich and H. A. Krieg, *J. Chem. Phys.,* 2010, **132**, 154104.

[70] G. Kresse and J. Hafner, *Phys.Rev. B.,* 1993, **47**, 558-561.

[71] G. Kresse and J. Furthmüller, *Comput. Mat. Sci.,* 1996, **6**, 15-50.
[72] G. Kresse and J. Furthmüller, *Phys.Rev. B.,* 1996, **54**, 11169-11186.
[73] J. P. Perdew, K. Burke. K. and M. Ernzerhof. *Phys. Rev. Lett.,* 1996, **77**, 3865–3868.
[74] P. E. Blöchl, *Phys. Rev. B.,* 1994, **50**, 17953-17979.
[75] G. Kresse and D. Joubert, *Phys.Rev. B.,* 1999, **59**, 1758-1775.
[76] F. Aquilante, J. Autschbach, R. K. Carlson, L. F. Chibotaru, M. G. Delcey, L. De Vico, I. F. Galván, N. Ferré, L. M. Frutos, L. Gagliardi, M. Garavelli, A. Giussani, C. E. Hoyer, G. L. Manni, H. Lischka, D. X. Ma, P. Malmqvist, T. Müller, A. Nenov, M. Olivucci, T. B. Pedersen, D. L. Peng, F. Plasser, B. Pritchard, M. Reiher, I. Rivalta, I. Schapiro, J. Segarra-Martí, M. Stenrup, D. G. Truhlar, L. Ungur, A. Valentini, S. Vancoillie, V. Veryazov, V. P. Vysotskiy, O. Weingart, F. Zapata and R. Lindh, *J. Comput. Chem.,* 2016, **37**, 506−541.
[77] B. O. Roos, P. R. Taylor, P. E. M. Siegbahn, *Chem. Phys.,* 1980, **48**, 157-288.
[78] P. A. Malmqvist, B. O. Roos and B. Schimmelpfennig, *Chem. Phys. Lett.,* 2002, **357**, 230−240.
[79] P. A. Malmqvist, B. O. Roos, *Chem. Phys. Lett*., 1989, **155**, 189−194.
[80] L. F. Chibotaru, L. Ungur, *J. Chem. Phys.,* 2012, **137**, 064112–064122.
[81] L. F. Chibotaru, L. Ungur. A. Soncini. *Angew. Chem., Int. Ed.,* 2008, **47**, 4126–4129.
[82] F. Aquilante, P.-A. Malmqvist, T. B. Pedersen, A. Ghosh and B. O. Roos, *J. Chem. Theory Comput.,* 2008, **4**, 694–702.
[83] B. O. Roos, R. Lindh, P.-A. Malmqvist, V. Veryazov and P.-O. Widmark, *J. Phys. Chem. A,* 2004, **108**, 2851–2858.
[84] B. O. Roos, R. Lindh, P.-A. Malmqvist, V. Veryazov and P.-O. Widmark. *J. Phys. Chem. A,* 2005, **109**, 6575–6579.
[85] B. O. Roos, R. Lindh, P.-A. Malmqvist, V. Veryazov, P.-O. Widmark and A.-C. Borin, *J. Phys. Chem. A,* 2008, **112**, 11431–11435.

Entry for the Table of Contents

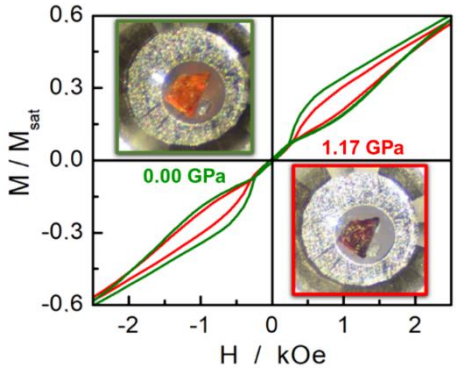

The Single-Molecule Magnet behaviour of an isotopically enriched dysprosium piezochromic mononuclear complex was modulated by applying an external pressure.

@PointillartF
@BGuennic
@chimie_ISCR